J. Fluid Mech. (1975), *vol.* 69, *part* 4, *pp.* 753–781
Printed in Great Britain

Turbulent convection in water over ice

By R. J. ADRIAN
Department of Physics, University of Cambridge†

(Received 30 May 1974)

Measurements have been made of the vertical velocity and simultaneous temperature fluctuation at fixed points in turbulent, statistically steady convection in water over an ice surface. Convection was confined to a horizontal layer of constant depth that lay under a stably stratified layer. Measurements of vertical velocities less than 1 mm/s were accomplished using a laser-Doppler velocimeter with a frequency-shifted reference beam. Vertical profiles of all relevant one-point moments, including joint temperature–velocity moments, up to third order were obtained. In the stable layer internal gravity waves were observed, and certain aspects of their behaviour were found to agree with existing theoretical analyses. Typical r.m.s. values of the temperature and velocity fluctuations were nearly equal to the appropriate 'convection' scales in the convection layer while in the conduction layer immediately above the ice surface they were more nearly equal to the 'molecular' scales. All of the observations were consistent with the existence of buoyant plume-like masses which dominated the structure of the flow. An analysis of the data using a conditional averaging technique to determine the mean properties of these masses showed that below the stable layer they accounted for over 80 % of the mean-square fluctuations in temperature and velocity.

1. Introduction

Thermal convection in water near its freezing point is distinguished from more common convective systems by the fact that the density of water attains a maximum value at a temperature $\theta_m = 3{\cdot}98\,^{\circ}\mathrm{C}$, thereafter decreasing with decreasing temperature according to the relationship

$$\rho' = \rho_m[1-\beta(\theta'-\theta_m)^2], \tag{1}$$

which is accurate to within 4 % between 0 and 8 °C when $\rho_m = 1{\cdot}0000\,\mathrm{g/cm^3}$, $\beta = 8{\cdot}1\times10^{-6}\,^{\circ}\mathrm{C}^{-2}$ and θ' is temperature. Thus, in a horizontal layer of water confined between a lower surface at a temperature less than θ_m and a warmer upper surface, the fluid below θ_m is unstably stratified, and it will undergo free convective motions if the layer depth is sufficiently large. The conditions for instability in terms of a critical modified Rayleigh number have been determined from linear stability analysis by Veronis (1963) and Sun, Tien & Yen (1969), who

† Present address: Department of Theoretical and Applied Mechanics, University of Illinois at Urbana-Champaign, Urbana, Illinois 61801.

have also determined the critical Rayleigh number experimentally for several combinations of upper and lower boundary temperatures (see also Yen 1968).

The behaviour of convection in water when the lower surface is at 0 °C (or more generally, less than 3·98 °C) and the upper surface is warmer than 3·98 °C is of special interest because the system divides into a convection layer lying under a stable layer. Veronis (1963) has shown that this system is subject to finite amplitude subcritical instabilities, and that motions in the convection layer can penetrate a finite distance into the region of stably stratified fluid. While studies of convection in water over ice are directly relevant to problems involving the melting of ice, additional attention has been focused on it as a simple means of analytically and experimentally studying the general phenomenon of penetrative convection, which plays a significant role in several important geophysical flows. Examples are the lifting of a nocturnal inversion layer in the atmosphere (Ball 1960; Lilly 1968; Deardorff, Willis & Lilly 1969), convection under the thermocline in the upper ocean (Phillips 1966, p. 2) and stellar convection (Leighton 1963).

Since Veronis' (1963) initial work more detailed analyses of convection in water over ice have been performed by Musman (1968) and Moore & Weiss (1973). In these studies two-dimensional flows with free boundaries were assumed and the maximum Rayleigh numbers were less than those required for transition to the turbulent flow regime. Steady-state flow solutions were obtained using the mean-field approximation (Herring 1963) in the former study, while in the latter the full governing equations were integrated numerically. Both analyses predicted horizontally periodic cells, and at large Rayleigh numbers Moore & Weiss (1973) observed cellular oscillations that were coupled to waves in the stable layer.

Experimental studies of convection in thin layers of water over ice have been performed by Tankin & Farhadieh (1971). The flows were laminar, and interferograms suggested periodic roll cells similar to those predicted by Musman (1968) and Moore & Weiss (1973) at low Rayleigh numbers. In the experiments of Townsend (1964) and Myrup *et al.* (1970) the layer depth was much larger ($\sim$ 10–15 cm), and the convection layer was turbulent. In both investigations dye-streak experiments showed that intermittent narrow plumes that extended across the convection layer were the prevalent structures, rather than roll cells. In addition, structures with 'dome shaped' heads similar in appearance to thermals were observed during the birth of a plume. Townsend (1964) found that sudden cooling of the lower plate in his box experiment produced a convection layer that grew upwards and eventually reached a constant depth that was determined essentially by the requirement that the conductive heat flux through the stable layer be equal to the turbulent heat flux in the convection layer. The latter quantity was independent of the convection-layer depth, as in Rayleigh convection where the heat flux is controlled by the conduction layer. One of Townsend's (1964) most interesting observations concerned the large magnitudes of temperature fluctuations near the interface between the convection layer and the stable layer. He attributed them to breaking internal gravity waves generated in the stable layer by the impact of rising fluid on its base. Wavelike motions have also been observed in convection in water over ice by Myrup *et al.* (1970) and

Moore & Weiss (1973), and in unsteady convection under a stable layer by Deardorff *et al.* (1969). Townsend (1964, 1966) showed that such waves would be confined to a thin layer above the interface, provided that the impact times of the rising fluid were long, as observed experimentally.

Results are reported here of an extension of the experiments of Townsend (1964) and Myrup *et al.* (1970) in which attention was limited to the statistically steady case, viz. constant interface height. The main objectives of the experiment were to examine the structure of the interfacial region for the purposes of testing Townsend's (1966) theory of the behaviour of the internal gravity waves and of better defining the turbulence dynamics at the interface. The primary new contributions of the present work are the addition of vertical velocity data, and a more accurate, detailed specification of the turbulent temperature fluctuations. In § 5 vertical profiles of the mean temperature, the mean density, the r.m.s. values of the fluctuating vertical velocity, temperature and density, the velocity–temperature correlation coefficient, the turbulent diffusion of thermal variance and kinetic energy of the vertical component and the skewness of velocity and temperature fluctuations are presented. In addition to yielding insight into the interfacial dynamics, the data also reveal the presence of organized, coherent structures in the underlying convection layer. Properties of these structures are discussed in § 6, where the data have been analysed using a conditional averaging technique.

2. Apparatus and instrumentation

Test section

The test section was a 33·3 × 33·3 cm square chamber formed by a 0·318 cm thick Dural lower plate, a parallel 0·636 cm thick Dural upper plate located 17·0 cm above the horizontal chamber floor and 0·636 cm thick Perspex side walls. The temperature of the lower plate was maintained at $-0{\cdot}1 \pm 0{\cdot}1$ °C by direct contact with coolant flowing under it through a nested system of counterflow channels. Freezing was observed in only one run (*C*), during which a 1 mm thick ice layer gradually built up over a 36 h period. A similar system maintained a constant upper plate temperature in the range 23–34 °C with an accuracy of $\pm 0{\cdot}02$ °C, and the temperature uniformity across both plates was better than 0·02 °C. The test section was surrounded by 10 cm thick styrofoam insulation along the side walls, and estimated heat losses through the sides were less than 5 % of the vertical heat flux. The arrangement is shown in figure 1.

Three sets of data, labelled *A*, *B* and *C*, were taken in steady-state convection with upper plate temperatures of 23·3, 25·6 and 33·7 °C respectively. Different upper plate temperatures produced slightly different convection-layer thicknesses as shown by the mean temperature profiles in figure 2. To assure steady-state conditions during the measurements the system was allowed to equilibrate for at least four hours after a nominally steady-state mean temperature profile had been achieved.

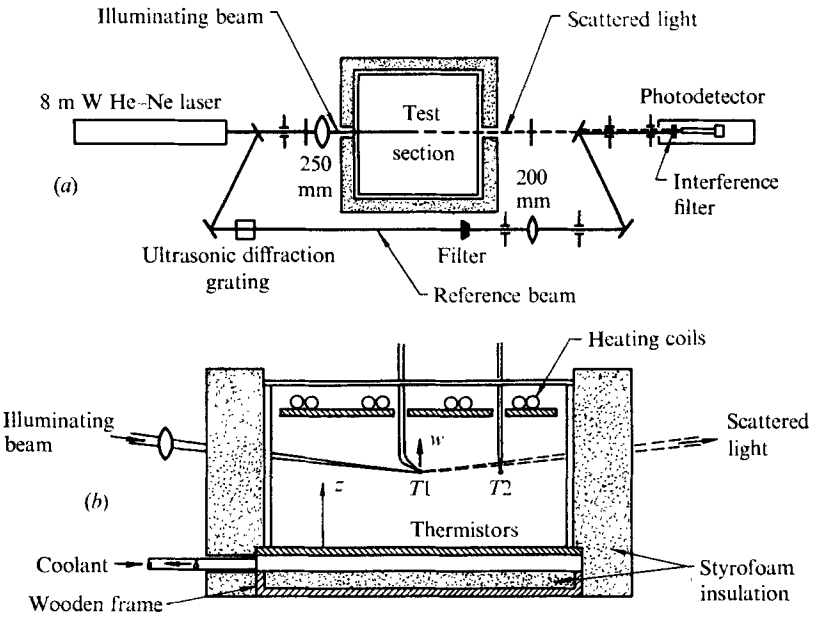

FIGURE 1. Test section, temperature sensors and schematic diagram of laser-Doppler velocimeter (upper and lower plate temperature sensors not shown). (*a*) Plan view. (*b*) Side view.

Temperature measurement

Local instantaneous temperatures were measured by sensor $T1$, a thermistor bead 0·02 cm in diameter located in the centre of the test section on the tip of a tapered glass tube. The tube was bent at an angle of 45° in order to reduce probe support interference with the vertical velocity. The thermistor's vertical position was adjustable with an accuracy of 0·005 cm, and its frequency response in water exceeded 10 Hz. A second sensor $T2$ was located about 10 cm away from $T1$, and was used to determine the horizontal uniformity of the mean temperature. Upper and lower plate temperatures were monitored by embedded thermistors. Linearized voltage output signals were obtained by placing the thermistors in specially constructed resistance bridges, and were calibrated against a certified mercury-in-glass thermometer at the beginning and end of the experiments. The calibrations were reproducible over the range of measurement to within 0·02 °C over a six-month period, and the equivalent noise input of sensor $T1$ was less than 0·01 °C.

Vertical velocity measurement

The reference-beam laser-Doppler velocimeter shown in figure 1 was arranged to measure the vertical component of velocity in a $0{\cdot}11 \times 0{\cdot}015 \times 0{\cdot}015$ cm measurement volume that had been located 0·2–0·3 cm to one side of sensor $T1$ in order to reduce probe interference with the vertical velocity. The laser light was scattered by a 0·002 % suspension of 0·5 μm polystyrene spheres (specific gravity 1·04), and its frequency was Doppler shifted by 5·55 kHz $(\mathrm{cm/s})^{-1}$ in the direction of observation. The sign and magnitude of the Doppler shift were detected by

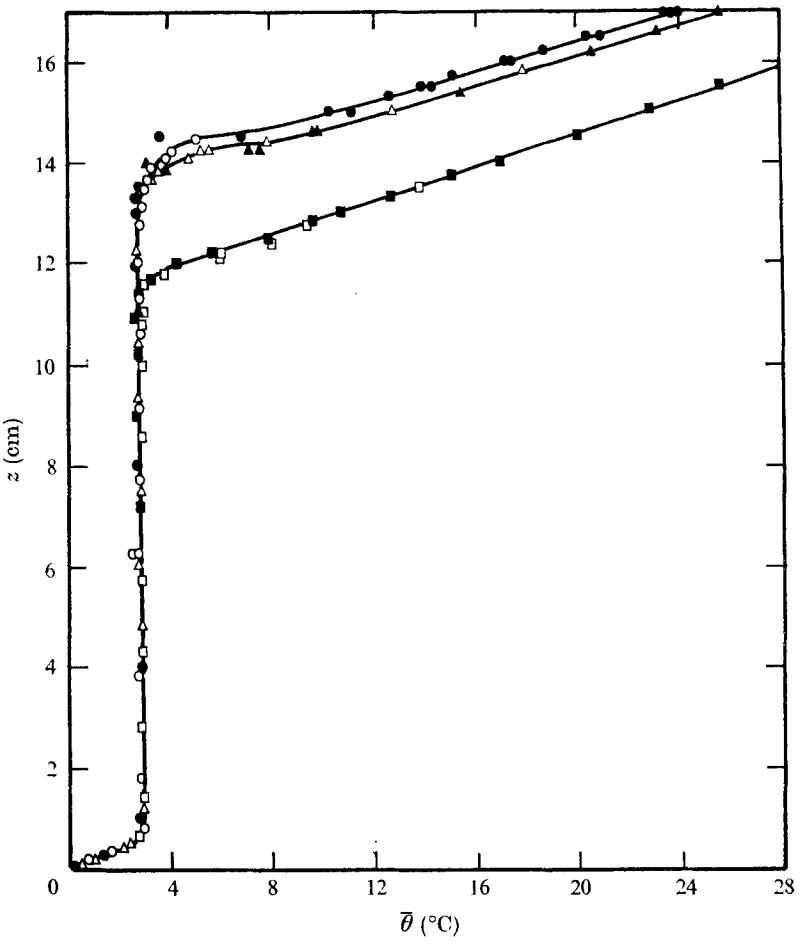

FIGURE 2. Mean temperature profiles in steady-state conditions. Filled symbols, sensor $T2$; open symbols, sensor $T1$. ○, run A; △, run B; □, run C.

optically mixing the scattered light on the photocathode of a photomultiplier tube with a reference beam that had been frequency shifted by $-8{\cdot}000000$ mHz so that the frequency shift appeared as a small deviation about an 8 mHz carrier. The frequency of the photocurrent was subsequently mixed down to a more convenient 50 kHz carrier frequency and converted to a voltage by a phase-locked loop. The frequency response of the system was determined by a 2 Hz bandwidth low-pass filter at the output. With this bandwidth the equivalent noise input was a constant, 0·0045 cm/s, arising primarily from random phase fluctuation in the laser output beam. Ambiguity phase fluctuations due to turbulent velocity gradients (George & Lumley 1973) were negligible.

The voltage output of the laser-Doppler velocimeter signal processing system was calibrated against the known velocity of a rotating liquid-filled wheel. Over the range of measurement ($\pm 0{\cdot}2$ cm/s) the voltage output was linearly related to the velocity, but was less than that expected from a calculation based on the

wheel velocity, the theoretical Doppler shift and the frequency–voltage calibration of the phase-locked loop. This effect was caused by low photocurrent signal-to-noise ratios (Adrian 1974). In addition, a d.c. voltage drift equivalent to $\pm 0{\cdot}01$ cm/s about the nominal zero-velocity value was observed. In reducing the velocity data, all values of the indicated fluctuating velocity were calculated as deviations from the time-averaged value of the indicated velocity in order to remove d.c. drift errors. The true velocity fluctuations w have been obtained by multiplying the indicated fluctuations by a factor of $1{\cdot}51$, which was determined from calibration at the signal-to-noise ratio typically obtained during the experiments. In certain instances, i.e. when the signal-to-noise ratio varied, this procedure produced errors of the order of 20 %, but corrections have not been made because the signal-to-noise ratio of the photocurrent was not monitored consistently throughout the experiments. An analysis of the effect of the signal-to-noise ratio, together with a more detailed description of the optical system and the signal processing system, has been presented elsewhere (Adrian 1974).

Data collection and analysis

The temperature data from $T1$ and the velocity data were digitized at a 0·25 Hz sampling rate. A short digitization time delay of the velocity sample compensated for the unequal frequency responses of the two sensors. With few exceptions all data records were at least 20 min long, and a typical data run, comprising one vertical profile, required 24–36 h. Even with such long record lengths, statistical sampling errors constituted a major source of uncertainty, but longer sampling times were not considered feasible. The data were analysed on a digital computer, and time averages over individual records, hereafter denoted by an overbar, were used to estimate mean values. Fluctuations of all quantities were defined as deviations from their time averages. Thus, the fluctuating velocity, temperature and density were calculated from

$$w = w' - \overline{w}, \quad \theta = \theta' - \overline{\theta}, \quad \rho = \rho' - \overline{\rho}, \tag{2}$$

where primes denote total values. Moments involving the vertical velocity were corrected for their random noise content by assuming that the noise in the velocity data was uncorrelated with either w or θ and had zero skewness. The r.m.s. value of the noise in the velocity data was taken to be 0·0045 cm/s for all runs. Corresponding corrections for noise in the temperature data were negligible.

A separate on-line sampling digital voltmeter was used to obtain the mean temperature from $T2$ and the two plate temperature sensors. The unit sampled data at a rate of 1 Hz and calculated the mean value for 1024 samples.

3. Statistical homogeneity in horizontal planes

The degree to which the experimental flow approached a horizontally homogeneous convective field was examined carefully, primarily because this condition was necessary to ensure that one-point time-averaged moments measured in the centre of the test section corresponded to horizontally averaged moments, and

therefore depended only on the height. Although the temperatures of the horizontal boundaries were very uniform and side-wall heat losses were small, horizontal homogeneity was not guaranteed *a priori* because the aspect ratio of the convection layer (ratio of width to depth) was only about 3 : 1. As was discussed by Thomas & Townsend (1957) and Deardorff & Willis (1967), side-wall effects in Rayleigh convection may produce large-scale mean circulations which in turn result in atypical data if measurements are made at fixed points. In the present experiments examinations of the mean temperature and velocity data did not provide conclusive evidence with regard to the homogeneity of the flow. Non-vanishing mean vertical velocities were observed at the centre of the test section, but only 3 % of the measured mean values fell outside the d.c. drift error band about the nominal zero-velocity value. Similarly, differences in the mean temperatures measured by sensors $T1$ and $T2$ were generally less than the sampling error, especially for run C, as shown by the data in figure 2. In addition, the linearity of the mean temperature profiles in the stable layer was consistent with vanishing horizontal heat fluxes. (In runs A and B the apparent increase in the mean temperature gradient above the base of the stable layer, followed by a decrease to a well-defined value further into the stable layer, was attributed to a slight thickening of the convection layer during the experiments.)

Measurements of vertical turbulent heat flux were more sensitive to the presence of mean flows and did suggest their existence. In general, the total vertical heat flux H was given by

$$H = \rho c_p(\overline{w}\overline{\theta} + \overline{w\theta} - \kappa\, d\overline{\theta}/dz), \tag{3}$$

where κ is the thermometric conductivity. Values of the total heat flux, given in table 1, were calculated from the mean temperature gradients at the upper plate, and the vertical heat fluxes were assumed to be constant and equal to those values at all heights. Within experimental error the values did not vary between runs and agreed well with Townsend's (1964) value of 34 mW cm^{-2}. In the core of the convection layer molecular heat conduction was negligible, so that in the absence of mean vertical velocities the total heat transfer should have equalled the turbulent heat-transfer term $\rho c_p \overline{\theta w}$ in (3). It was found, in fact, that the measured values of the turbulent heat transfer were only 50, 45 and 93 % of the total heat transfer in runs A, B and C, respectively. Since spuriously low values of the temperature–velocity correlation caused by probe separation and interference could not account for more than half of the discrepancies in the magnitude of the heat flux in runs A and B, it was concluded that significant fractions of the vertical heat flux were due to mean vertical flows. The velocities of such flows need not have been large: a value of $\overline{w} = 0{\cdot}0015$ cm/s could have accounted for the entire discrepancy observed in run B. Although these results suggest caution in the interpretation of the statistics obtained from the single-point data and time averaging, it does not appear that the moments other than $\overline{\theta w}$ were overly sensitive to the lack of horizontal homogeneity. The moment data from runs A and B were in substantial agreement with those from run C, even though mean flow fields were apparently much smaller in the latter experiment.

Run	H (mW/cm^2)	z_* (cm)	w_* (cm/s)	θ_* (°C)	z_0 (cm)	w_0 (cm/s)	θ_0 (°C)
A	35·4	14·15	0·0521	0·155	0·0897	0·0148	0·548
B	36·0	13·95	0·0524	0·157	0·0902	0·0148	0·550
C	34·2	11·80	0·0490	0·160	0·0915	0·0146	0·539

TABLE 1

4. Non-dimensionalization

The data have been made dimensionless by use of either the 'molecular' scales for convection in water over ice (Townsend 1964)

$$w_0 = (\kappa\beta g Q^2)^{\frac{1}{5}}, \quad z_0 = \kappa/w_0, \quad \theta_0 = Q/w_0, \tag{4}$$

or the 'convection' scales, given by

$$w_* = (\beta g z_* Q^2)^{\frac{1}{4}}, \quad z_*, \quad \theta_* = Q/w_*. \tag{5}$$

In these formulae κ is the thermometric conductivity, β is defined in (1), g is the acceleration due to gravity and Q is the kinematic heat flux,

$$Q = H/\rho c_p. \tag{6}$$

Physically, the convection length scale z_* is the depth of the convection layer, and for present purposes it has been defined as the height at which the mean temperature reached 3·98 °C. Values of the scales are given in table 1.

In the derivation of the molecular scales the fundamental assumptions are that in certain regions of the flow the convection-layer depth is not dynamically significant, but molecular diffusion is important. Hence the molecular scales are expected to be appropriate in boundary regions such as the conduction layer and the interfacial layer. Corresponding scales for fluids having linear temperature–density relationships have been derived by Thomas & Townsend (1957), and have been shown to produce similarity scaling in the conduction layer over a single heated plate (Townsend 1959). The convection scales for water over ice are analogous to the scales proposed by Deardorff (1969) for convection in air. In contrast to the molecular scales, they are intended to apply in regions where the length scale of the convective motion is of the order of the layer depth and molecular diffusion is not important, i.e. in the core of the convection layer.

While various modified Rayleigh numbers can be defined for convection in water over ice (Veronis 1963; Tien 1968), they are basically related to the stability of the system and probably do not provide a basis for comparisons with turbulent Rayleigh convection. A more appealing approach in terms of readily interpreted turbulence quantities can be developed by using the length scales defined above. It may be shown that the molecular length scale z_0 is of the order of the Kolmogorov microscale, and it has been implicitly assumed that the convection length scale z_* is a measure of the integral length scale. Consequently, the scale ratio z_*/z_0 is a measure of the 'degree of turbulence' in the sense that large scale

ratios imply many degrees of freedom. An alternative interpretation of the scale ratio is obtained by noting that the convection Péclet number, defined as

$$Pe_* = w_* z_*/\kappa, \tag{7}$$

is related to the scale ratio by

$$Pe_* = (z_*/z_0)^{\frac{4}{3}} \tag{8}$$

for convection in water over ice. A similar relation applies to Rayleigh convection except that the exponent in (8) is replaced by $\frac{4}{3}$ and the length scales are replaced by those appropriate to convection in fluids with linear density–temperature relationships. Some indication of the degree of turbulence in convection in water over ice is obtained by postulating dynamic similarity with Rayleigh convection either on the basis of equal scale ratios or equal convection Péclet numbers (equal convection Reynolds numbers are a third possibility). For example, in run *C* the length-scale ratio was $z/z_* = 129$ and the convection Péclet number was $Pe_* = 435$. In Rayleigh convection in water the same value of the scale ratio occurs at a Rayleigh number of $4{\cdot}7 \times 10^9$, while the same value of Pe_* occurs at a Rayleigh number of about 1×10^8. On either basis the equivalent Rayleigh number was several orders of magnitude greater than the value for transition to turbulent flow ($Ra \approx 50\,000$), and it is concluded that the flow in the present experiments was well into the turbulent regime.

5. Unconditionally averaged moments

Mean temperature and density

Profiles of the dimensional mean temperature have been presented in figure 2, and details of the non-dimensional profile are shown in figure 3. A cold layer of narrow extent wherein heat was transferred primarily by conduction was observed above the lower plate. Following Kraichnan (1962), the height z_κ at which the heat transferred by conduction was equal to the turbulent heat transfer has been used as a quantitative indicator of the conduction-layer thickness. It may be shown that in horizontally homogeneous convection with constant heat flux z_κ is also the height at which the production term in the equation for the time evolution of temperature variance (Deardorff & Willis 1967) is a maximum. In the present experiments $z_\kappa \simeq 4{\cdot}5 z_0$, which was somewhat larger than either the typical value $z_\kappa \simeq 3z_0$ found by Townsend (1959) in air or the value $z_\kappa \simeq 3{\cdot}5 z_0$ calculated from Chu & Goldstein's (1973) data for water at $Ra = 1{\cdot}86 \times 10^7$.

The mean temperature gradient vanished slightly above the conduction layer at about $10z_0$ and again at about $12z_0$, below the interface between the convection layer and the stable layer. Between these two levels, i.e. in the core of the convection layer, a small reversed mean temperature gradient occurred in the form of a nominally linear decrease in the mean temperature from a maximum value of 2·92 °C to a minimum value of 2·78 °C. A reversed gradient of comparable magnitude appeared to be present in the central core region in the experiments of Townsend (1964) and Myrup *et al.* (1970), but in the former experiments considerably stronger reversals occurred in relatively narrow layers at the edges of the

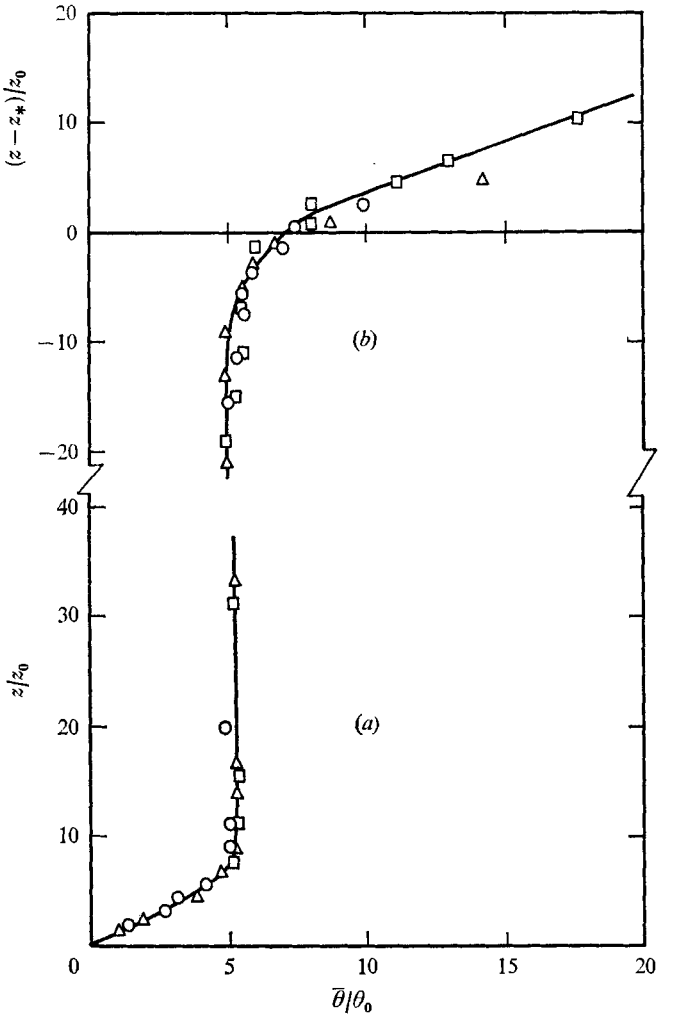

FIGURE 3. Non-dimensional mean temperature profiles. (*a*) Conduction layer. (*b*) Interfacial region. ○, run *A*; △, run *B*; □, run *C*.

convection layer, resulting in peak mean temperature 'overshoots' of about 0·3 °C. In addition, the mean temperature in the middle of the convection layer was almost 0·4 °C warmer in Townsend's (1964) experiments than in the present ones. Gradient reversals were predicted by the analyses of Musman (1968) and Moore & Weiss (1973), but while Musman's results showed an overshoot near the interface and no overshoot above the conduction layer, Moore & Weiss predicted the converse situation. The large mean temperature overshoots in Townsend's (1964) experiments may have been caused by a tongue of ice that covered about the middle two-thirds of the lower plate and may, quite plausibly, have driven a mean circulation in the form of downflow along the side walls and upflow in the centre of the tank.

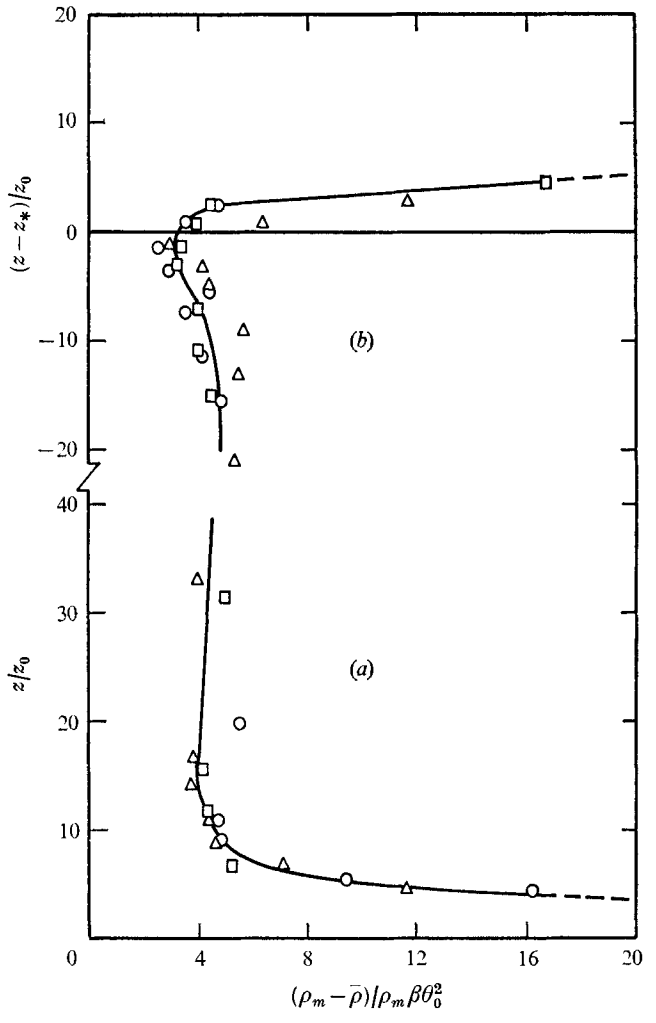

FIGURE 4. Non-dimensional mean density profiles. (*a*) Conduction layer. (*b*) Interfacial layer. ○, run *A*; △, run *B*; □, run *C*.

The dimensionless profile of mean density is shown in figure 4, where $\bar{\rho}$ has been calculated from the temperature data and the time average of (1),†

$$\bar{\rho} = \rho_m[1-\beta(\bar{\theta}-\theta_m)^2-\beta\tilde{\theta}^2]. \tag{9}$$

The data demonstrate the strongly unstable density stratification in the conduction layer, and the comparably strong stable stratification in the stable layer. In the convection-layer core the stratification was slightly stable, except for a small region extending about 10–$15z_0$ below the interface. Stable stratification in the core was associated almost entirely with the reversed mean temperature gradient, whereas unstable stratification immediately below the stable layer was caused by the increase in the density of water near 3·98 °C. As expected, a relative

† A tilde will be used throughout to denote a r.m.s. value.

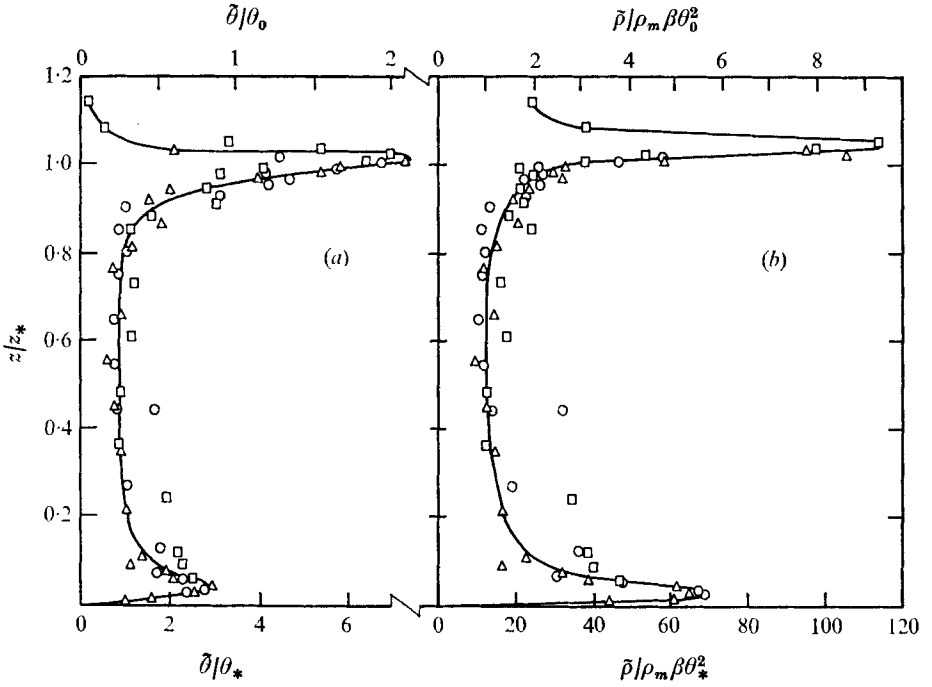

FIGURE 5. (*a*) Profile of non-dimensional r.m.s. temperature fluctuation data. (*b*) Profile of non-dimensional r.m.s. density fluctuation data calculated from (10). Upper scales pertain to run *C* data only. ○, run *A*; △, run *B*; □, run *C*.

maximum in the density profile occurred close to 3·98 °C, but owing to the $\tilde{\theta}^2$ term in (9) the maximum possible density ρ_m was never achieved. Consequently fluid elements having temperatures close to 3·98 °C were negatively buoyant in the interfacial region.

Second-order moments

The profiles of r.m.s. temperature and density fluctuations in figure 5 (*a*) and (*b*) have been made dimensionless by the convection temperature scale and plotted against z/z_* to facilitate comparisons. The molecular scalings at the top of the figures were calculated for only the run *C* data, but were nearly correct for runs *A* and *B* as well. In the conduction layer $\tilde{\theta}$ reached a maximum value of $0{\cdot}85\theta_0$ at a height of about $5z_0$, which nearly coincided with the height of maximum production of temperature variance. Townsend (1959) found that peak values of $\tilde{\theta}$ occurred somewhat lower, at $z \simeq 3z_0$. The r.m.s. temperature fluctuation assumed a nearly constant value of $0{\cdot}9\theta_*$ in the convection-layer core, and attained a second relative maximum at a level just slightly above the interface. Peak interfacial values of $\tilde{\theta}$ were approximately 2·5 times larger than the peak conduction-layer values, compared with a ratio of 1·6 inferred from Townsend's (1964) data on peak-to-peak temperature fluctuations.

Root-mean-square fluctuations in the density were calculated from the temperature data and the formula

$$\tilde{\rho} = \rho_m\beta[4(\overline{\theta}-\theta_m)^2\tilde{\theta}^2 + 4(\overline{\theta}-\theta_m)\overline{\theta^3} + \overline{\theta^4} - \tilde{\theta}^4]^{\frac{1}{2}}, \tag{10}$$

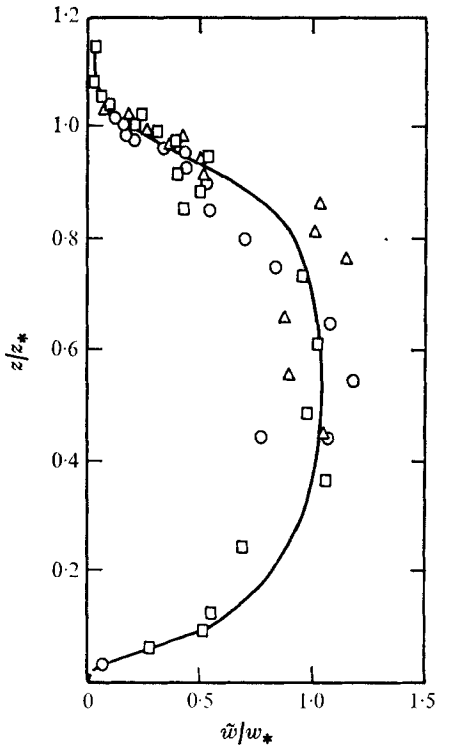

FIGURE 6. Non-dimensional profile of r.m.s. vertical velocity. ○, run *A*; △, run *B*; □, run *C*.

which follows directly from (1) and the definition of the density fluctuations [cf. (2)] by time averaging. In the Boussinesq approximation for incompressible fluids ρg represents the buoyancy force, and the profiles in figure 5 may be interpreted as the r.m.s. buoyancy forces made dimensionless by a buoyancy scale based on either θ_0 or θ_*. The values of the buoyancy force were largest in relatively thin regions within the conduction layer and the interfacial layer, and decreased rapidly in the stable layer. Contributions to the profile peaks were made by both positive and negative density fluctuations, but positively buoyant fluid tended to make the dominant contribution in the conduction layer while negatively buoyant fluid dominated above z_* in the interfacial layer. Compared with the peak in the $\tilde{\theta}$ profile the level of the maximum density fluctuations was shifted upwards into the stable layer. The shift resulted primarily from increasing values of $\overline{\theta}-\theta_m$ above the base of the stable layer, and large peak values of $\tilde{\rho}$ indicated the strongly decelerating buoyancy force experienced by fluid that had penetrated into the stable layer.

The r.m.s. vertical velocity profile shown in figure 6 clearly shows that small vertical motions extended at least a distance $0{\cdot}1z_*$ into the stable layer. In $0{\cdot}85 < z/z_* < 0{\cdot}95$ there was a tendency for the data to remain constant, but since there was no convincing reason for such behaviour, a smooth line with no plateau has been drawn through the data. In the core of the convection layer

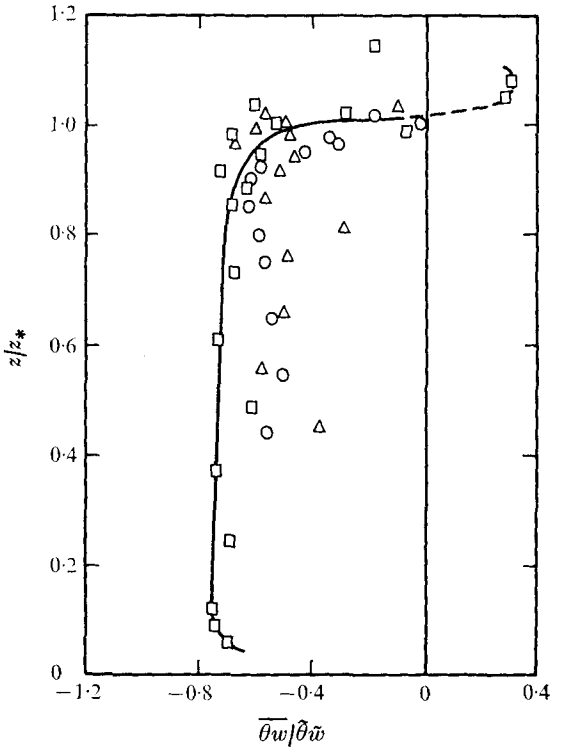

FIGURE 7. Profile of the temperature–vertical velocity correlation coefficient. ○, run *A*; △, run *B*; □, run *C*.

the vertical gradients of $\tilde{w}$ were small, and the average value of $\tilde{w}/w_*$ in $0{\cdot}3 < z/z_* < 0{\cdot}8$ was approximately unity. The relative paucity of velocity data in the lower regions of the convection layer prevented a detailed comparison with the results of other investigations, but the profile was roughly similar to those measured by Deardorff & Willis (1967). In the conduction layer at $z = z_\kappa$ the value of the transition Péclet number $Pe_T = \tilde{w}z_\kappa/\kappa$ was very close to the value of 3·0 assumed by Kraichnan (1962) in his mixing-length theory.

The temperature–velocity correlation coefficients, shown in figure 7, were scattered, but behaved in a manner that was consistent with the mean temperature profiles and the condition of constant heat flux. Above $z/z_* \simeq 1{\cdot}05$ both $\overline{\theta w}$ and $\tilde{w}$ were small, and consequently the magnitudes of the correlation coefficients were unreliable. In addition, the two positive values in the stable layer were dubious, although counter-gradient heat fluxes may conceivably have been expected in this region by anaolgy with the results of Deardorff *et al.* (1969). In view of the discussion in §3, the $\overline{\theta w}$ data from run *C* were considered to be the most reliable, and the solid line sketched through the data was heavily weighted towards the run *C* results, which indicated a constant correlation coefficient of about $-0{\cdot}75$ in the convection layer. This behaviour seemed more reasonable than a dip in the correlation coefficient in the core, as suggested by the data from runs *A* and *B*, but it may be noted that such a dip was observed by Deardorff &

Willis (1967) in Rayleigh convection at a Rayleigh number of 10^7. For comparison, the vertical average of all of the correlation coefficients measured by Deardorff & Willis (1967) was $0{\cdot}58 \pm 0{\cdot}03$ for $6{\cdot}3 \times 10^5 < Ra < 1{\cdot}0 \times 10^7$.

Internal gravity waves

A basic assumption in Townsend's (1964, 1966) analyses of the internal gravity waves in the stable layer was that the waves were of small amplitude. Under this assumption the temperature and velocity fluctuations are related by

$$\dot{\theta} + w\, d\overline{\theta}/dz = 0, \tag{11}$$

where the dot denotes partial differentiation with respect to time and molecular conduction has been neglected in the enthalpy equation (Lamb 1932, p. 378). An immediate consequence of (11) is

$$\tilde{w} = \frac{\tilde{\dot{\theta}}}{d\overline{\theta}/dz}. \tag{12}$$

Measured values of $\tilde{w}/w_0$ are compared in figure 8 with the values predicted from (12) using measurements of $\tilde{\dot{\theta}} = (\overline{\dot{\theta}^2})^{\frac{1}{2}}$ and $d\overline{\theta}/dz$ to evaluate its right-hand side. (The values of $\tilde{\dot{\theta}}$ were calculated from the curvature of the temperature autocorrelation at zero time lag.) Within experimental uncertainty the comparison indicates that the wave amplitudes were small at heights above $z - z_* = -4z_0$. Below this level the predicted values became very large because $d\overline{\theta}/dz$ was approaching zero while $\tilde{\dot{\theta}}$ remained finite, obviously a finite amplitude effect.

It may be shown that Townsend's (1966) analysis predicts the following asymptotically valid power laws for the r.m.s. vertical velocities in the stable layer:

$$\tilde{w} = \begin{cases} \text{constant}\ (z - z_*)^{-\frac{1}{4}}, & 0 < z - z_* \ll z_c, \qquad (13\,a) \\ \text{constant}\ (z - z_*)^{-\frac{25}{12}}, & z_c \ll z - z_*. \qquad (13\,b) \end{cases}$$

The $-\frac{1}{4}$ power decay in (13 *a*) results from the nonlinear density stratification immediately above the interface, while the much more rapid decay predicted by (13 *b*) is caused by viscous damping of the wave motions. The critical depth is given by

$$z_c = \left(\frac{a^6}{8\beta^3 g^3 (d\overline{\theta}/dz)_\infty^6\, \nu^2 \tau^8} \right)^{\frac{1}{5}}, \tag{14}$$

where a is the typical horizontal extent of a penetrating column of fluid, τ is the typical duration of the impact, $(d\overline{\theta}/dz)_\infty$ is the constant temperature gradient in the stable layer and ν is the kinematic viscosity.

Townsend's power laws are compared with the measurements of the dimensionless r.m.s. vertical velocity in figure 9. Agreement with (13 *b*) is reasonably good far into the stable layer, but below the critical depth the data varied more slowly than the $-\frac{1}{4}$ power law predicted by (13 *a*). The discrepancy may have resulted from curvature in the experimental mean temperature profiles below $z - z_* = 3z_0$, since Townsend (1966) assumed that the temperature gradient was a constant equal to $(d\overline{\theta}/dz)_\infty$ for $z > z_*$. Figure 9 suggests that $z_c \simeq 3z_0$, and experimentally

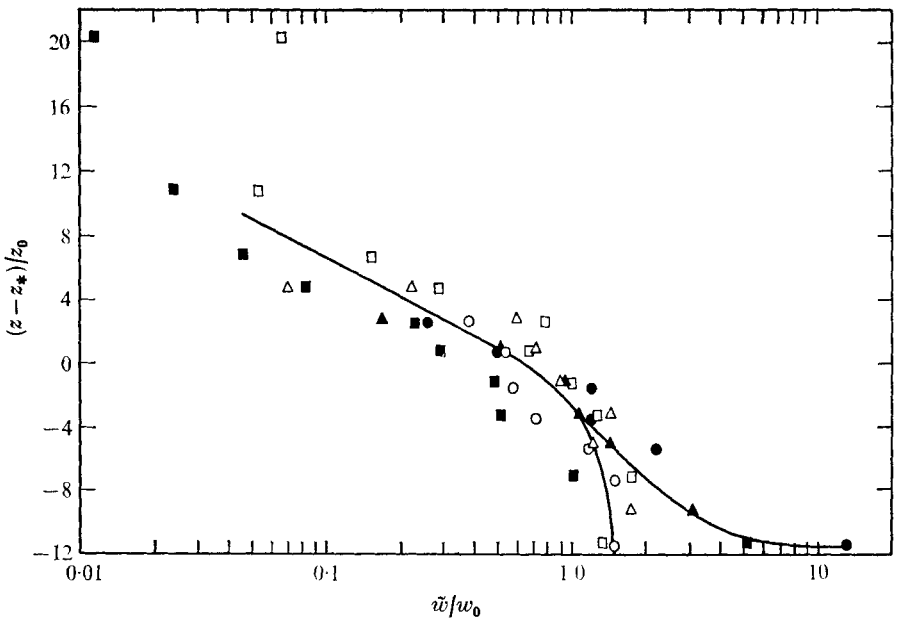

FIGURE 8. Comparison of measured r.m.s. vertical velocity data (open symbols) in the interfacial region with the values predicted by (12) (closed symbols). ○, run *A*; △, run *B*; □, run *C*.

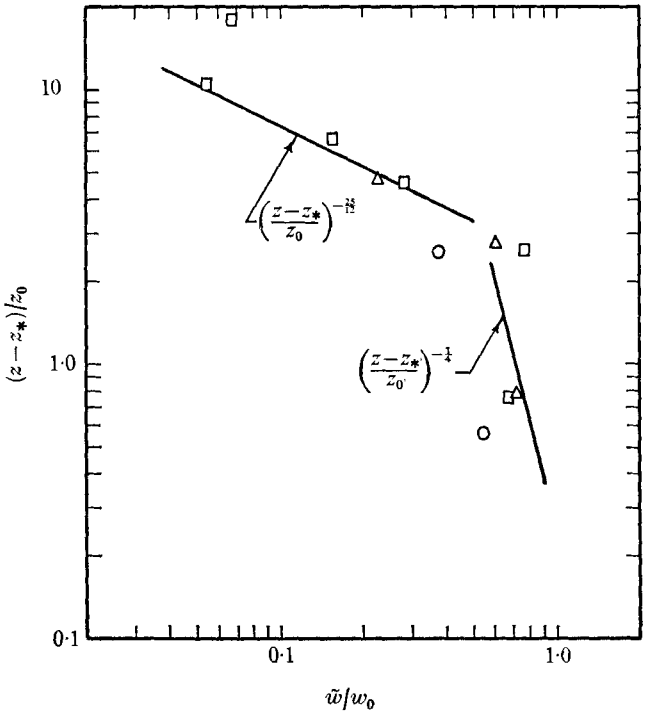

FIGURE 9. Comparison of the r.m.s. vertical velocity data in the stable layer with the asymptotic decay laws predicted by Townsend (1964). ○, run *A*; △, run *B*, □, run *C*.

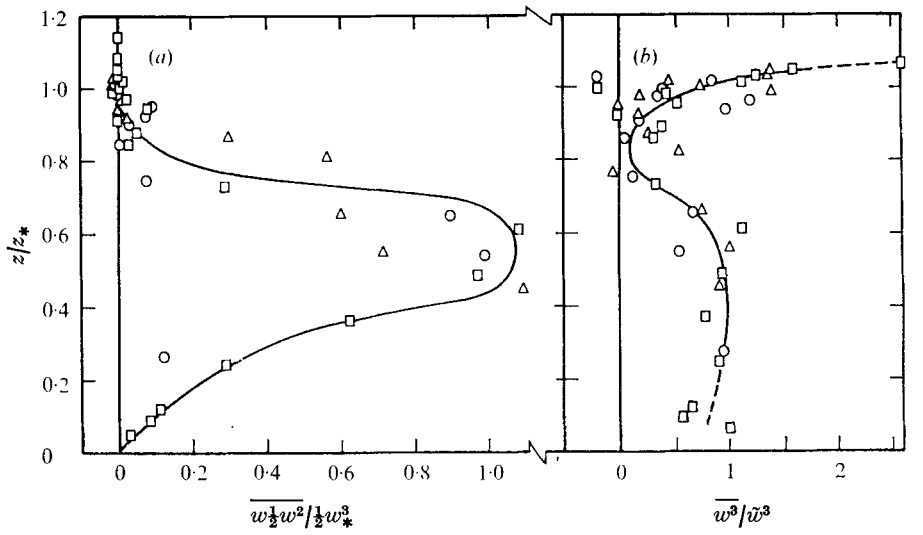

FIGURE 10. (*a*) Non-dimensional turbulent diffusion of kinetic energy in the vertical velocity component. (*b*) Skewness of the vertical velocity fluctuations. ○, run *A*; △, run *B*; □, run *C*.

it was found that the temporal microscale of the temperature fluctuations, defined as

$$\tau_\theta = \tilde{\theta}/\tilde{\theta}, \tag{15}$$

was about 20 s at $z = z_*$. Using these values as estimates of z_c and τ, equation (14) predicted that the horizontal extent of the 'ripples' caused by impinging fluid columns was $a \approx 3{\cdot}5$ cm at the interface. Townsend's (1966) estimates for z_c, τ and a were $4{\cdot}4z_0$, 10 s and 1·5 cm, respectively.

Third-order moments

The mean cubed velocity in the form $\overline{w\frac{1}{2}w^2}/w_* \frac{1}{2}w_*^2$ represents the dimensionless diffusion of kinetic energy in the vertical velocity component by fluctuations in the vertical velocity. The negative of its vertical derivative corresponds to the net upward diffusion, and is one of several similar energy diffusion terms that appear in the equation for mean turbulent kinetic energy. In general the vertical diffusion (figure 10*a*) was positive, indicating that on average the largest fluctuations in the vertical velocity were of positive sign. Diffusion was largest near the middle of the convection layer, where the net diffusion vanished, and the net diffusion was always away from the core of the convection layer, i.e. generally down the vertical gradient of $\frac{1}{2}\tilde{w}^2$. Both the diffusion and its derivative were small and vanished smoothly above $z/z_* \simeq 0{\cdot}9$.

The velocity skewness data, shown in figure 10 (*b*), reached a nearly constant value close to unity in the core of the convection layer. Above $z/z_* \simeq 0{\cdot}6$ the skewness decreased to a minimum value close to zero at about $z/z_* = 0{\cdot}85$, and then increased rapidly to relatively large values in the stable layer. Although the numerator and denominator were small in the stable layer, the increasing trend

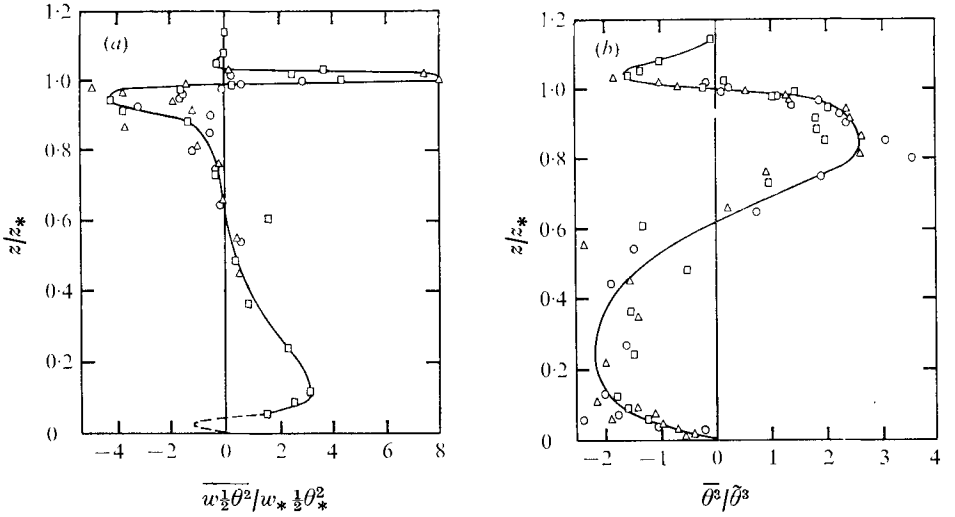

FIGURE 11. (*a*) Non-dimensional turbulent diffusion of the temperature variance. (*b*) Skewness of the temperature fluctuations. ○, run *A*; △, run *B*; □, run *C*.

was felt to be a real manifestation of relatively energetic ascending fluid penetrating into the stable layer.

The thermal analogues of the quantities in figure 10 are the dimensionless diffusion of thermal variance $\overline{w\frac{1}{2}\theta^2}/w_*\,\frac{1}{2}\theta_*^2$, representing the transport of temperature fluctuation variance by vertical velocity fluctuations, and the skewness of the temperature fluctuations. The profiles of these quantities, shown in figures 11(*a*) and (*b*) respectively, exhibited marked relationships between themselves and with the velocity skewness profile. Both thermal quantities attained large peak values having opposite signs in the lower regions of the convection layer, and changed sign almost simultaneously at $z/z_* \simeq 0{\cdot}6$, coinciding with the height at which the velocity skewness began to decrease. Above $z/z_* \simeq 0{\cdot}6$ large relative maxima having opposite signs were again attained, followed by a very rapid decrease in magnitude and change in sign at $z/z_* \simeq 0{\cdot}99$. Within the stable layer very large positive peak values of the diffusion of temperature variance occurred, and were associated with large negative peak values of the temperature skewness. In this region the qualitative dissimilarity between the widths of the peaks in the two profiles was primarily the consequence of normalizing the mean cubed temperature by $\tilde{\theta}^3$. Profiles of $\overline{\theta^3}/\theta_*^3$ exhibited sharp peaks immediately above and below the interface whose widths were comparable with those of the peaks in the $\overline{w\frac{1}{2}\theta^2}/w_*\,\frac{1}{2}\theta_*^2$ profile. In addition, the magnitude of the peak value of $\overline{\theta^3}/\theta_*^3$ in the stable layer was much larger than either of the peak values that occurred below the interface; for example, $\overline{\theta^3}/\theta_*^3 \simeq 300$ at $z/z_* \simeq 1{\cdot}03$ compared with $\overline{\theta^3}/\theta_*^3 \simeq 130$ at $z/z_* \simeq 0{\cdot}97$ or $\overline{\theta^3}/\theta_*^3 \simeq 25$ at $z/z_* \simeq 0{\cdot}06$.

The behaviour of the second- and third-order moments was determined primarily by two dominant mechanisms that can be seen in the sequence of representative temperature and velocity records shown in figure 12. Note that the fluctuations have been normalized by their r.m.s. values, and that $-w/\tilde{w}$ has

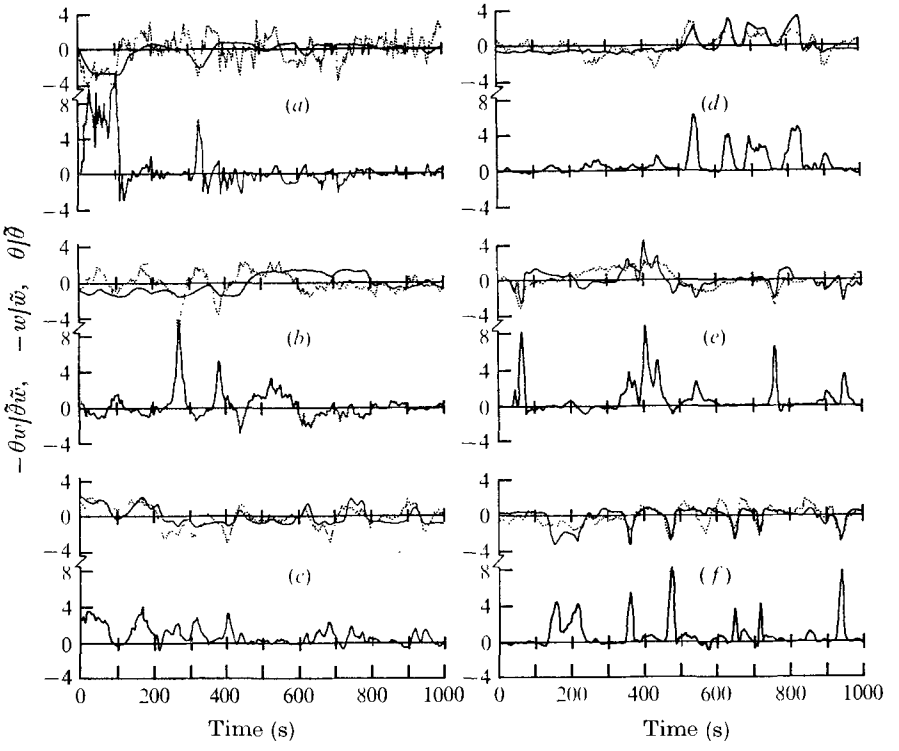

FIGURE 12. Records of the fluctuating temperature, vertical velocity and instantaneous heat flux. Upper plots: ——, $\theta/\tilde{\theta}$; ·····, $-w/\tilde{w}$. Lower plot: ——, $-\theta w/\tilde{\theta}\tilde{w}$.

(*a*)	$z/z_* = 1{\cdot}036$,	$\bar{\theta} = 6{\cdot}01$ °C,	$\tilde{\theta} = 0{\cdot}86$ °C,	$\tilde{w} = 0{\cdot}004$ cm/s.
(*b*)	$z/z_* = 1{\cdot}020$,	$\bar{\theta} = 4{\cdot}30$ °C,	$\tilde{\theta} = 1{\cdot}11$ °C,	$\tilde{w} = 0{\cdot}011$ cm/s.
(*c*)	$z/z_* = 0{\cdot}975$,	$\bar{\theta} = 3{\cdot}14$ °C,	$\tilde{\theta} = 0{\cdot}50$ °C,	$\tilde{w} = 0{\cdot}019$ cm/s.
(*d*)	$z/z_* = 0{\cdot}914$,	$\bar{\theta} = 3{\cdot}01$ °C,	$\tilde{\theta} = 0{\cdot}48$ °C,	$\tilde{w} = 0{\cdot}019$ cm/s.
(*e*)	$z/z_* = 0{\cdot}647$,	$\bar{\theta} = 2{\cdot}86$ °C,	$\tilde{\theta} = 0{\cdot}12$ °C,	$\tilde{w} = 0{\cdot}056$ cm/s.
(*f*)	$z/z_* = 0{\cdot}120$,	$\bar{\theta} = 2{\cdot}93$ °C,	$\tilde{\theta} = 0{\cdot}35$ °C,	$\tilde{w} = 0{\cdot}027$ cm/s.

been plotted in order to facilitate visual comparison with $\theta/\tilde{\theta}$. The first mechanism was most evident just above the conduction layer (figure 12*f*), and took the form of large, intermittent, positive vertical velocity fluctuations that were almost always accompanied by large, equally intermittent, negative temperature fluctuations. This mechanism was evident with somewhat variable clarity throughout the convection layer. In order to demonstrate the close correlation between large velocity and large temperature fluctuations, the instantaneous kinematic turbulent heat flux $\overline{\theta w}$ has been normalized by $-\tilde{\theta}\tilde{w}$ and plotted below the velocity–temperature records. The instantaneous heat flux was generally small and varied randomly about zero, except for relatively short periods during which values up to ten times the local mean turbulent heat flux were caused by simultaneously large negative temperatures and positive vertical velocities. These heat-flux pulses presumably resulted from the passage of ascending fluid masses that had been ejected from the conduction layer. The second mechanism was a mirror image of the first. It was most easily discerned below the interface

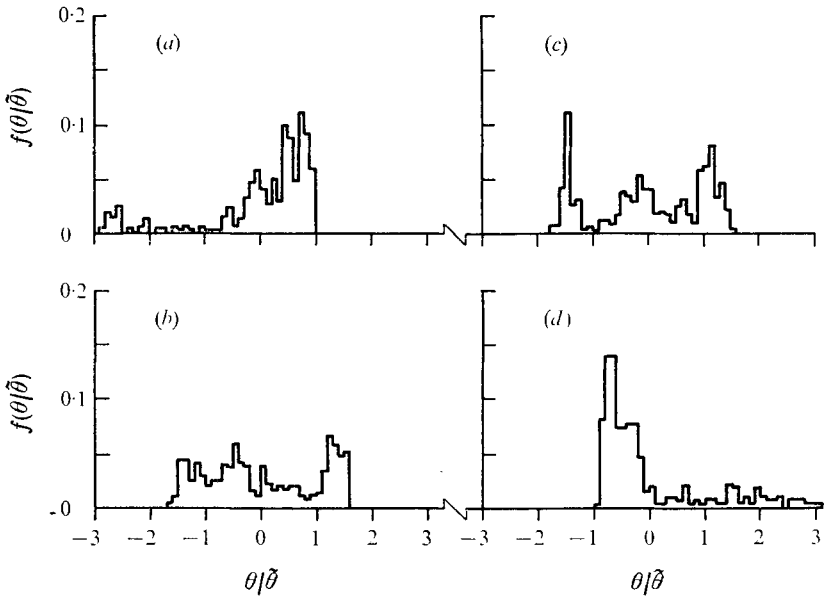

FIGURE 13. Probability density histograms of temperature fluctuations in the interfacial region.

(*a*) $z/z_* = 1{\cdot}036$, $\bar{\theta} = 6{\cdot}01$ °C, $\tilde{\theta} = 0{\cdot}86$ °C.
(*b*) $z/z_* = 1{\cdot}020$, $\bar{\theta} = 4{\cdot}30$ °C, $\tilde{\theta} = 1{\cdot}11$ °C.
(*c*) $z/z_* = 1{\cdot}005$, $\bar{\theta} = 4{\cdot}30$ °C, $\tilde{\theta} = 1{\cdot}02$ °C.
(*d*) $z/z_* = 0{\cdot}990$, $\bar{\theta} = 3{\cdot}22$ °C, $\tilde{\theta} = 0{\cdot}65$ °C.

(figure 12*d*), where large positive fluctuations of the temperature and large negative fluctuations of the velocity produced large pulses of turbulent heat flux interspersed by relatively inactive periods. The generation of these fluctuations was attributed to warm fluid masses descending from the stable layer.

In general, both mechanisms coexisted in combinations of varying strength (cf. figures 12*c*, *e*) and the strength of one relative to the other determined the sign and magnitude of the third-order moments. Thus, below $z/z_* \simeq 0{\cdot}6$ cold ascending fluid masses were dominant, resulting in negative temperature skewness, positive velocity skewness and positive diffusion of temperature variance. A similar situation occurred above the interface, where the cold rising fluid generated large negative temperature fluctuations as it penetrated into the warm stable layer. In $0{\cdot}6 < z/z_* < 0{\cdot}98$ the flow statistics were dominated by warm descending fluid masses and hence the temperature skewness was positive and diffusion of temperature variance was negative. The velocity skewness was reduced to a small value in this region by the opposing contributions of the positive and negative velocities (cf. figure 12*c*). In general, vanishing values of the diffusion of temperature variance and temperature skewness occurred at heights where the opposing velocity–temperature characteristics of the two mechanisms cancelled on average.

The transition from dominance of one mechanism to dominance of the other is demonstrated in figure 13 by the sequence of probability density histograms for

temperature fluctuations in the interfacial region for run C. Above the interface (figure 13 a) small positive fluctuations were most probable, but infrequent negative fluctuations with magnitudes up to $-3\tilde{\theta}$ (2·6 °C) occurred with sufficient frequency to result in a net negative skewness. The reverse situation existed below the interface, as shown in figure 13 (d). Slightly above the interface, see figures 13 (b) and (c), $\tilde{\theta}$ was a maximum, and the frequencies of occurrence of fluctuations with either large positive amplitudes or large negative amplitudes were approximately equal. The presence of two distinct mechanisms was manifested by the bimodal side lobes of the distribution in figure 13 (c). Similar probability densities were found for runs A and B.

6. Conditionally averaged statistics

Coherent and incoherent fluid

The results discussed above combined with the flow-visualization studies of Townsend (1964) and Myrup *et al.* (1970) led naturally to a simplified physical model of turbulent convection in water over ice in which the flow field characteristically contained organized structures which will be referred to here as 'coherent'. For convenience the fluid inside a coherent structure will be called 'coherent fluid', while that lying outside will be called 'incoherent fluid'. Within the coherent structures the deviations from the mean vertical velocity and temperature were large and made large negative contributions to the mean (negative) turbulent heat flux. Ascending coherent fluid was cold, and it apparently originated in the unstable conduction layer, from which it was intermittently ejected at a rate that may have been determined by conduction-layer growth and decay times as in the models proposed by Howard (1966) and Foster (1971). Following a transient post-ejection phase (during which the ejected fluid probably had the appearance of a thermal or a starting plume) the ascending coherent fluid assumed a tall columnar shape which extended across the convection layer and persisted until the conduction layer at its base was locally depleted of buoyant fluid. The results also clearly indicated the presence of descending coherent fluid but the flow-visualization studies did not provide much insight into the shape of such structures. Descending coherent fluid was warm, and hence negatively buoyant in the convection layer, and its most likely site of production was the interfacial layer. Unlike the ascending coherent fluid, the mechanism for the production of descending coherent fluid may not have been related simply to local stability because the unstable density stratification around the interface was relatively weak. In terms of this model incoherent fluid was the more or less passive fluid that separated the two types of coherent fluid, and its contributions to the flow statistics were generally small in magnitude.

The concepts of coherent and incoherent fluid correspond in several ways to those of 'active' and 'quiescent' fluid introduced by Townsend (1959), but some distinctions do exist. For example, in figure 12 (d) the temperature fluctuations during the time interval 230–320 s would have been called quiescent in Townsend's (1959) terminology, but would probably be classified as ascending coherent fluid in the present model. The existence of ascending coherent struc-

tures in convection in water over ice is clearly a phenomenon that is quite similar to the thermals that have been observed in the planetary boundary layer (Priestley 1959, p. 67) and, in a more general sense, to the structural 'bursts' of low-momentum fluid found in wall regions of isothermal turbulent boundary layers (Kline *et al.* 1967; Corino & Brodkey 1969; Willmarth & Lu 1972).

Conditional sampling criteria

In order to evaluate quantitatively the importance of the coherent fluid mechanisms, the data were statistically analysed using a conditional sampling criterion based on the instantaneous turbulent heat flux to distinguish between coherent and incoherent fluid. Specifically, it was assumed that coherent fluid was present whenever the instantaneous heat flux was sufficiently large and of the same sign as the mean turbulent heat flux, as suggested by the curves in figure 12. Data points in the θ, w plane were classified into five groups according to the following inequalities:

$$\left.\begin{array}{lll} \text{(I)} & \theta > 0, & w > 0 \\ \text{(II)} & \theta > 0, & w < 0 \\ \text{(III)} & \theta < 0, & w < 0 \\ \text{(IV)} & \theta < 0, & w > 0 \end{array}\right\} \quad \text{and} \quad |\theta w| > F\tilde{\theta}\tilde{w}, \tag{16}$$

$$\text{(V)} \quad |\theta w| < F\tilde{\theta}\tilde{w}.$$

Data in groups II and IV represented descending and ascending coherent fluid, respectively, while groups I and III represented incoherent fluid. Group V contained those points whose membership in any other group could not be ascertained with certainty because of either experimental errors or inherent defects in the sampling criterion. The value of F effectively set a discrimination level, and while the quantitative results were not insensitive to F, variations in its value over a reasonable range did not substantially alter their qualitative behaviour. Large values of F left very few data points in regions I–IV, while very small values provided no discrimination against inaccurate classification. Hence, a compromise value of $F = 0{\cdot}1$ was used to calculate all of the results to be presented. This value was satisfactory except above the interface, where noise fluctuations in the vertical velocity signal were a significant fraction of $\tilde{w}$. Conditionally averaged results in this region were generally meaningless and are not presented unless their trend is obvious. Had a substantially larger number of data samples been available, a somewhat greater value of F would have been preferable. It should also be remarked that the scatter in the conditionally sampled results was not small, and that a reasonable degree of latitude was exercised in arriving at the curves to be presented. In general, the trends and magnitudes of the results from individual runs agreed to within 30 %, but in some regions the error bounds were larger. While alternative sampling criteria could have been devised, the present method (which was analogous to the one used by Willmarth & Lu (1972) in the turbulent boundary layer) probably provided as sharp a distinction between coherent and incoherent fluid as could reasonably have been expected from single-point data.

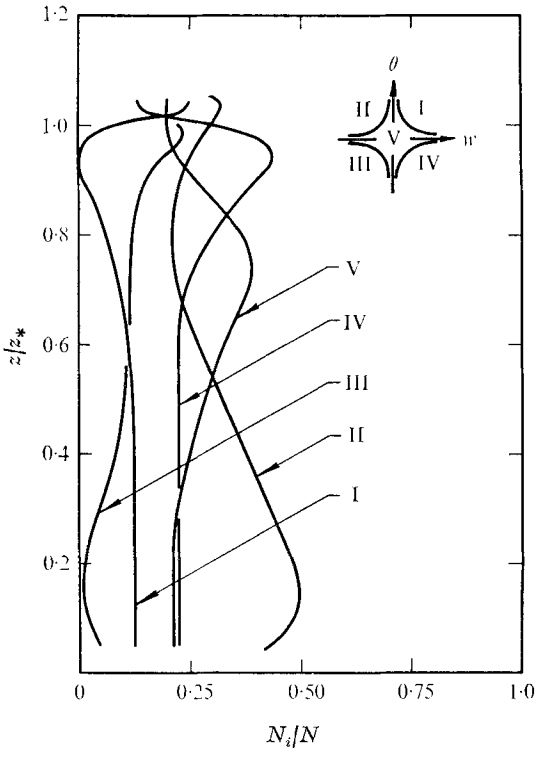

FIGURE 14. Relative frequency of data points in groups I–V. $F = 0{\cdot}1$.

Profiles of the relative frequency of data points in groups I–V are shown in figure 14, where N_i = number of samples in the ith group and N = total number of samples. Assuming that single-point time averages were equivalent to horizontal averages, the quantity N_i/N also represented the average horizontal area occupied by fluid in the ith group. Ascending coherent fluid (IV) occupied approximately 20 % of the horizontal area up to $z/z_* \simeq 0{\cdot}6$. Between this level and the stable layer the area reached a maximum of about 45 %, reflecting in part horizontal spreading of the ascending fluid as it approached the interface. Coherent descending fluid (II) also appeared to spread horizontally as the conduction layer was approached from above. In addition to horizontal spreading, some of the variations in the curves of N_i/N were caused by conversion of fluid from one group to another. For example, some of the cold descending incoherent fluid (III) may have been fluid that had been entrained near the interface and dragged downwards by descending coherent fluid. While traversing the convection layer the entrained fluid would have been warmed by contact with the warmer coherent fluid, and conversely portions of the coherent descending fluid would have cooled. Thus after a time some fraction of each group would have been converted to fluid in group V, possibly accounting for part of the relative maximum in the N_V/N curve at $z/z_* \simeq 0{\cdot}75$ and the preceding decreases in the N_{II}/N and N_{III}/N curves starting at $z/z_* \simeq 1$. At still lower heights the remaining warm coherent fluid would have gradually converted entrained fluid belonging

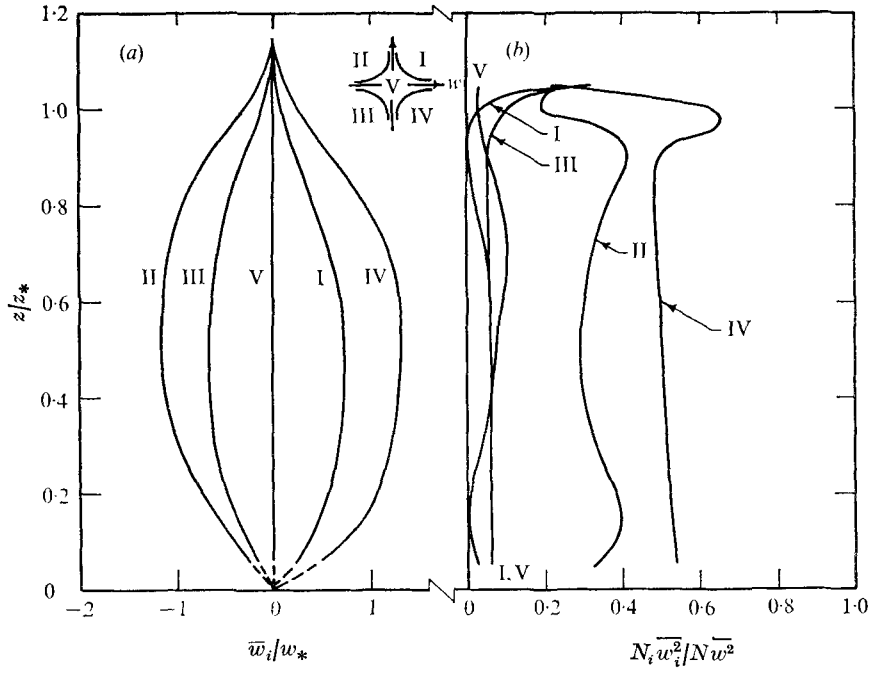

FIGURE 15. (*a*) Conditionally averaged mean vertical velocities. (*b*) Fraction of the variance of the vertical velocity component associated with groups I–V. $F = 0{\cdot}1$.

to groups III and V into group II fluid, thereby diminishing N_{III}/N and N_{V}/N as observed below $z/z_* \simeq 0{\cdot}6$. A similar sequence of events involving group I fluid entrained by ascending coherent fluid may have produced the minimum in N_{I}/N near $z/z_* \simeq 0{\cdot}93$.

Conditional averages

Two types of conditional average have been calculated. Given any function $G(\theta, w)$ the conditional average $\overline{G}_i$ was the mean value of G for points belonging to the ith group:

$$\overline{G}_i = \frac{1}{N_i} \sum_{a \in i} G(\theta_a, w_a), \quad i = \mathrm{I}, \ldots, \mathrm{V}. \tag{17}$$

For example, $\overline{\theta}_{\mathrm{II}}$ was the mean deviation of the temperature of the descending coherent fluid from $\overline{\theta}$. The second type of average represented the fractional contribution made by the fluctuations in a given class of fluid to the total mean value of the fluctuation. It was related to the conditional average by

$$\frac{1}{N\overline{G}} \sum_{a \in i} G(\theta_a, w_a) = \frac{N_i}{N} \frac{\overline{G}_i}{\overline{G}}, \quad i = \mathrm{I}, \ldots, \mathrm{V}. \tag{18}$$

Profiles of the dimensionless conditionally averaged vertical velocity and the fractional contribution to the variance of the vertical velocity are shown in figures 15(*a*) and (*b*). Mean vertical velocities of the coherent fluid (II and IV) were of the order of $\pm 1{\cdot}2 w_*$ in the core of the convection layer and were approxi-

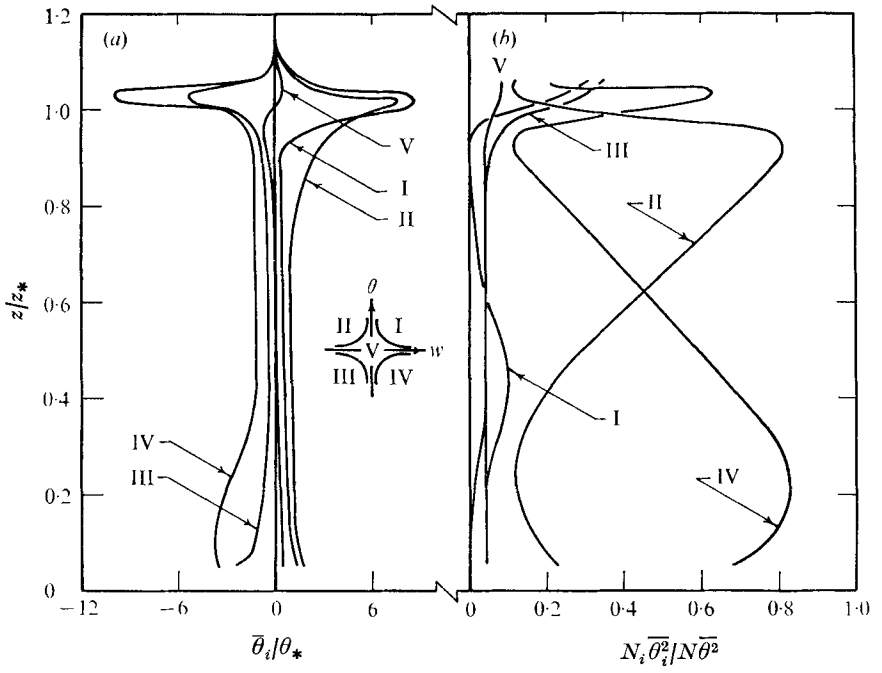

FIGURE 16. (*a*) Conditionally averaged mean temperatures. (*b*) Fraction of the variance of the temperature fluctuation associated with groups I–V. $F = 0{\cdot}1$.

mately twice as large as the mean velocities of the incoherent fluid (I and III). Below the stable layer ascending and descending coherent fluid accounted for roughly 50 % and 30–40 % of the vertical velocity variance, respectively. The rapid variations of the group II and group IV curves in figure 15(*b*) near the interface may have been spurious, but the tendency for the fractional contributions of all groups (except V) to equilibrate above the interface probably reflected the presence of internal gravity waves with uncorrelated velocity and temperature fluctuations.

The dimensionless mean temperature deviations are shown in figure 16(*a*). The mean temperature deficit of ascending coherent fluid (IV) was about $-4\theta_*$ just above the conduction layer, which was equivalent to $-1{\cdot}0\theta_0$. At $z/z_* \simeq 1{\cdot}02$ the mean temperature excess of descending coherent fluid (II) was a maximum value, about $8\theta_* \simeq 2\theta_0$ in magnitude. This corresponded to a typical temperature excess of ~ 1 °C over a local mean temperature of 4·5 °C, suggesting that descending coherent fluid typically originated around the 5·5 °C level. The decay in the curves for groups II and IV to values of the order of $1{\cdot}0\theta_*$ in the core of the convection layer was caused by heat transfer between the coherent fluid and adjacent fluid and indicated the rate of buoyancy loss as the coherent fluid traversed the convection layer. Large values of the mean temperature deficit of the ascending coherent fluid occurred above the interface and reached a maximum value of approximately $-10\theta_* \simeq -1{\cdot}5$ °C at heights where the local mean temperatures were between 5·5 and 6·5 °C. Since the temperature of ascending

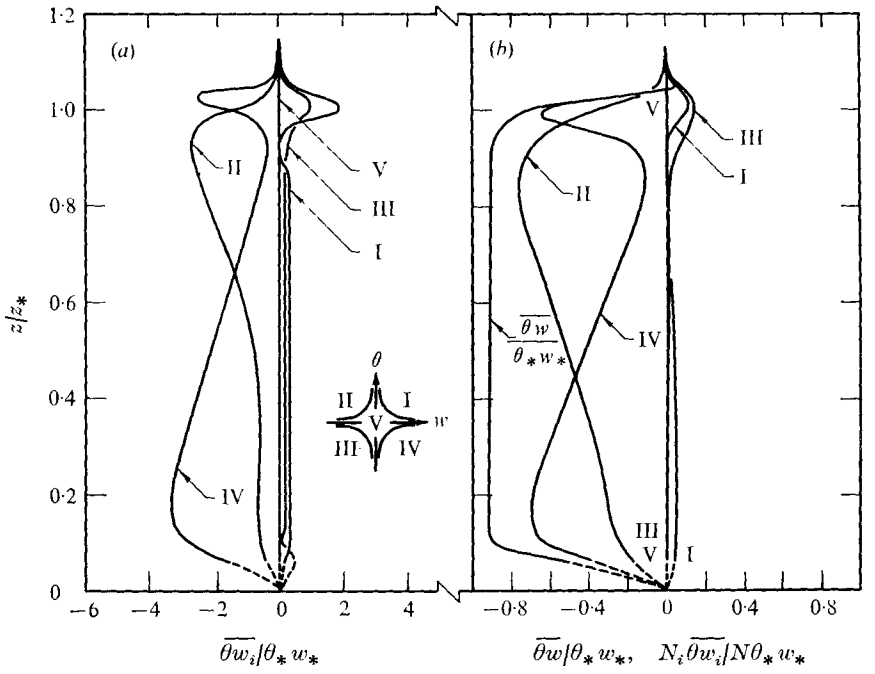

FIGURE 17. (*a*) Conditionally averaged mean heat fluxes. (*b*) Ratio of the measured turbulent heat flux to the total vertical heat flux and the turbulent heat flux associated with groups I–V normalized by the total vertical heat flux. $F = 0{\cdot}1$.

coherent fluid was not expected to be much above 3 °C after penetrating to this height, it appeared that some of the negative fluctuations at this level were associated with 4–5 °C interfacial fluid that had been pushed upwards by the impact of ascending coherent fluid.

The temperature fluctuations of the ascending coherent fluid accounted for over 80% of the total mean-square fluctuation just above the conduction layer, and those of the descending coherent fluid accounted for a nearly equal fraction just below the interface, as shown in figure 16 (*b*). The contributions from each mechanism decreased to small values of the order of 15 % at opposing sides of the convection layer, but at any height within the convection layer the combined contribution of groups II and IV, i.e. of all of the coherent fluid, amounted to 75–80 % of the total temperature variance. At the interface the descending and ascending coherent fluid contributed in nearly equal proportions to $\hat{\theta}^2$, while at larger heights the contribution of the ascending coherent fluid peaked at a value over 60 %, followed by a sharp decrease and a concomitant increase in the incoherent fluid contribution, consistent with the existence of internal gravity wave motion in the stable layer.

Plots of the conditional-averaging results for the turbulent heat fluxes are shown in figure 17. The profiles were based primarily on data from run *C*, since the measured values of $\overline{\theta w}$ agreed best with the total kinematic heat flux Q ($= \theta_* w_*$) in this run (cf. §3). The plot of $\overline{\theta w}/\theta_* w_*$ in figure 17 (*b*) shows that in the core of the convection layer $\overline{\theta w}/\theta_* w_*$ was about 0·93. As shown in figure 17 (*a*),

the conditionally averaged turbulent heat fluxes of the ascending and descending coherent fluid reached respective maximum values of 3·6 and 3·0 times the total heat flux at $z/z_* \simeq 0{\cdot}15$ and $z/z_* \simeq 0{\cdot}9$. Conditionally averaged incoherent heat fluxes were generally less than 15 % of these values everywhere except in the stable layer; $\overline{\theta w}_{\mathrm{V}}/\theta_* w_*$ was always negligible. The variations of the curves for the coherent fluid were primarily associated with the decay of coherent fluid temperature deviations, rather than varying mean velocities or horizontal areas. Typically, the values of $\overline{\theta w}_{\mathrm{II}}/\overline{\theta}_{\mathrm{II}}\overline{w}_{\mathrm{II}}$ and $\overline{\theta w}_{\mathrm{IV}}/\overline{\theta}_{\mathrm{IV}}\overline{w}_{\mathrm{IV}}$ averaged across the convection layer were $1{\cdot}06 \pm 0{\cdot}05$ and $1{\cdot}12 \pm 0{\cdot}05$, respectively (95 % confidence limits). The large mean temperature deficit of the ascending coherent fluid produced a large negative mean heat flux above the interface, but this was not significantly larger than the conditional mean values of the incoherent heat fluxes in this region.

In figure 17 (*b*) the profiles represent the fraction of the total heat flux associated with each of the five groups. The curves are such that

$$\sum_{i=\mathrm{I}}^{\mathrm{V}} N_i \overline{\theta w}_i / N\theta_* w_* = \overline{\theta w}/\theta_* w_*.$$

The locations of the relative maxima and general shapes of the curves are similar to those in figure 17 (*a*). Across the convection layer the individual coherent fluid heat fluxes varied from about $-0{\cdot}8\theta_* w_*$ to $-0{\cdot}2\theta_* w_*$, but the variation was such that the total heat flux associated with the coherent fluid was nearly constant. The opposing positive heat-flux contribution due to incoherent fluid (I and III) reached a maximum value of about $0{\cdot}35\theta_* w_*$ in the stable layer but below $z/z_* \simeq 0{\cdot}9$ its magnitude was always less than $0{\cdot}05\theta_* w_*$.

7. Summary and discussion

The results indicate that the structure of the turbulent convective field in the experiments was considerably less random than might have been expected, particularly in view of the relatively large effective Rayleigh numbers involved. The structured regions of the flow have been called 'coherent', and within the core of the convection layer the velocity and temperature fluctuations of the coherent fluid were nearly equal to the respective convection scales, suggesting that the (vertical) length scales of the coherent structures were of the order of z_*. Within the limits of the accuracy set by uncertainties inherent in the sampling criterion, the conditionally averaged data show that, depending on height, the coherent fluid (II plus IV) occupied between 40 and 70 % of the horizontal area, but accounted for 70–80 % of the magnitudes of the temperature and vertical velocity variances. Also, over most of the convection layer the magnitude of the turbulent heat flux due to coherent fluid was over twenty times greater than the incoherent fluid heat flux.

The observations suggest that it may be feasible to model many of the properties of convection in water over ice (and other types of convection) by essentially neglecting its turbulent character and modelling only the low wavenumber motions. Such models should be three-dimensional, satisfy no-slip

conditions at the boundaries, and should probably also be unsteady, since the production of coherent fluid is definitely intermittent. Moreover, it may be necessary to include interaction between the ascending and descending coherent fluid, especially in the regions of large coherent fluid production such as the conduction layer or the interfacial layer, where the arrival of ascending coherent fluid may have created descending coherent fluid by either a simple subsidence mechanism or by generating gravity waves that 'broke' during downward excursions. One of the existing models of convection in water over ice is steady (Musman 1968) and the other unsteady (Moore & Weiss 1973), but both assume two-dimensional flow with free-surface boundary conditions. Even so, many of the predicted properties appear to agree at least qualitatively with the observations, and more detailed quantitative comparisons would be useful.

With regard to statistical theories of turbulent convection, one consequence of the high degree of structure was that the statistics of the velocity and temperature fluctuations were always far from a joint normal distribution. Thus theories based on low-order expansions about a joint normal state, or on assumed quasi-normal higher-order moments may not yield good representations. On the other hand, it seems likely that the coherent fluid dominated the integral scales of length and time, as well as the transport properties of the convective field. In that case, the existence of prominent coherent structures actually provides some justification for mixing-length/relaxation-time models such as those of Lundgren (1969, 1971), Chung (1970), Adrian (1972) and Lumley & Khajeh-Nouri (1974), in which turbulent transport is attributed to motions having a single average length scale and relaxation time scale. It may, in fact, be conjectured that coherent structures are requisites for the success of such theories.

The author wishes to express his appreciation to Dr A. A. Townsend, who initially stimulated interest in the water over ice convection system and made many useful comments; to Mr G. Garner and Mr J. Burr, who skillfully constructed much of the experimental apparatus; and to Dr J. C. Mumford and Dr R. M. Thomas for their advice on the design of the electronics instrumentation. During the period of research reported here the author received support from the Winston Churchill Foundation of America.

REFERENCES

Adrian, R. J. 1972 Ph.D. thesis, Cambridge University.

Adrian, R. J. 1974 *Proc. 3rd Biennial Symp. on Turbulence in Liquids, Rolla, Missouri.* To appear.

Ball, F. K. 1960 *Quart. J. Roy. Met. Soc.* **86**, 483.

Chu, T. Y. & Goldstein, R. J. 1973 *J. Fluid Mech.* **60**, 141.

Chung, P. M. 1970 *Phys. Fluids*, **13**, 1153.

Corino, E. R. & Brodkey, R. S. 1969 *J. Fluid Mech.* **37**, 1.

Deardorff, J. W. 1969 *J. Atmos. Sci.* **27**, 1211.

Deardorff, J. W. & Willis, G. E. 1967 *J. Fluid Mech.* **28**, 675.

Deardorff, J. W., Willis, G. E. & Lilly, D. K. 1969 *J. Fluid Mech.* **35**, 7.

Foster, T. D. 1971 *Geophys. Fluid Dyn.* **2**, 201.

GEORGE, W. K. & LUMLEY, J. L. 1973 *J. Fluid Mech.* **60**, 321.

HERRING, J. R. 1963 *J. Atmos. Sci.* **20**, 325.

HOWARD, L. N. 1966 *Proc. 11th Int. Cong. Appl. Mech.* (ed. H. Görtler), p. 1109. Springer.

KLINE, S. J., REYNOLDS, W. C., SCHRAUB, F. A. & RUNSTADLER, P. W. 1967 *J. Fluid Mech.* **30**, 741.

KRAICHNAN, R. H. 1962 *Phys. Fluids*, **5**, 1374.

LAMB, H. 1932 *Hydrodynamics*. Dover.

LEIGHTON, R. B. 1963 *Annual Review of Astronomy and Astrophysics*, p. 19. Palo Alto: Annual Reviews, Inc.

LILLY, D. K. 1968 *Quart. J. Roy. Met. Soc.* **94**, 292.

LUMLEY, J. L. & KHAJEH-NOURI, B. 1974 *Adv. in Geophys.* A **18**, 169.

LUNDGREN, T. S. 1969 *Phys. Fluids*, **12**, 485.

LUNDGREN, T. S. 1971 *Phys. Fluids*, **14**, 225.

MOORE, D. R. & WEISS, N. O. 1973 *J. Fluid Mech.* **61**, 553.

MUSMAN, S. 1968 *J. Fluid Mech.* **31**, 342.

MYRUP, L., GROSS, D., HOO, L. S. & GODDARD, W. 1970 *Weather*, **25**, 150.

PHILLIPS, O. M. 1966 *The Dynamics of the Upper Ocean*. Cambridge University Press.

PRIESTLEY, C. H. B. 1959 *Turbulent Transfer in the Lower Atmosphere*. University of Chicago Press.

SUN, Z.-S., TIEN, C. & YEN, Y.-C. 1969 *A.I.Ch.E. J.* **15**, 910.

TANKIN, R. S. & FARHADIEH, R. 1971 *Int. J. Heat Mass Transfer*, **14**, 953.

THOMAS, D. B. & TOWNSEND, A. A. 1957 *J. Fluid Mech.* **2**, 473.

TIEN, C. 1968 *A.I.Ch.E. J.* **14**, 652.

TOWNSEND, A. A. 1959 *J. Fluid Mech.* **5**, 209.

TOWNSEND, A. A. 1964 *Quart. J. Roy. Met. Soc.* **90**, 248.

TOWNSEND, A. A. 1966 *J. Fluid Mech.* **24**, 307.

VERONIS, G. 1963 *Astrophys. J.* **137**, 641.

WILLMARTH, W. W. & LU, S. S. 1972 *J. Fluid Mech.* **55**, 65.

YEN, Y.-C. 1968 *Phys. Fluids*, **11**, 1263.